ADVANCED FUNCTIONAL MATERIALS

Postfach 10 11 61
69451 Weinheim
Germany
Courier services:
Boschstraße 12
69469 Weinheim
Germany
Tel.: (+49) 6201 606 531
Fax: (+49) 6201 606 500
E-mail: afm@wiley.com

WILEY-VCH

Dear Author,

Please correct your galley proofs carefully and return them no more than four days after the page proofs have been received.

Please limit corrections to errors already in the text; cost incurred for any further changes or additions will be charged to the author, unless such changes have been agreed upon by the editor.

The editors reserve the right to publish your article without your corrections if the proofs do not arrive in time.

Note that the author is liable for damages arising from incorrect statements, including misprints.

Please note any queries that require your attention. These are indicated with a Q in the PDF and a question at the end of the document.

Reprints may be ordered by filling out the accompanying form.

Return the reprint order form by fax or by e-mail with the corrected proofs, to Wiley-VCH : afm@wiley.com

To avoid commonly occurring errors, **please ensure that the following important items are correct** in your proofs (please note that once your article is published online, no further corrections can be made):

- **Names** of all authors present and spelled correctly
- **Titles** of authors correct (Prof. or Dr. only: please note, Prof. Dr. is not used in the journals)
- **Addresses** and **postcodes** correct
- **E-mail address** of corresponding author correct (current email address)
- **Funding bodies** included and grant numbers accurate
- **Title** of article OK
- All **figures** included
- **Equations** correct (symbols and sub/superscripts)

Corrections should be made directly in the PDF file using the PDF annotation tools. If you have questions about this, please contact the editorial office. The corrected PDF and any accompanying files should be uploaded to the journal's Editorial Manager site.

Author Query Form

WILEY

Journal ADFM

Article adfm202008088

Dear Author,

During the copyediting of your manuscript the following queries arose.

Please refer to the query reference callout numbers in the page proofs and respond.

Please remember illegible or unclear comments and corrections may delay publication.

Many thanks for your assistance.

Query No.	Description	Remarks
Q-license	Please note that the article can only be published once an appropriate license agreement has been signed. The responsible corresponding author will have received an e-mail invitation to register/log in and sign a license agreement in Wiley Author Services (https://authorservices.wiley.com). The costs of publishing this manuscript OnlineOpen might be covered by one of Wiley's national agreements. To find out more please visit, https://authorservices.wiley.com/authorresources/Journal-Authors/open-access/affiliation-policies-payments/index.html. Eligibility for fee coverage is determined by the affiliation of the responsible corresponding author.	
Q1	Please confirm that forenames/given names (blue) and surnames/family names (vermilion) have been identified correctly.	
Q2	Please provide the highest academic title (either Dr. or Prof.) for all authors, where applicable.	
Q3	Please define all acronyms at their first appearance in the abstract, text and table of contents, respectively. Only expanded forms are allowed if the elements are cited only once in the article.	
Q4	Please provide volume number for ref. [37], if now available.	

Please confirm that Funding Information has been identified correctly.

Please confirm that the funding sponsor list below was correctly extracted from your article: that it includes all funders and that the text has been matched to the correct FundRef Registry organization names. If a name was not found in the FundRef registry, it may not be the canonical name form, it may be a program name rather than an organization name, or it may be an organization not yet included in FundRef Registry. If you know of another name form or a parent organization name for a "not found" item on this list below, please share that information.

FundRef Name	FundRef Organization Name
King Abdullah University of Science and Technology	King Abdullah University of Science and Technology
Soonchunhyang University Research Fund	

K. J. Lee, B. Turedi, A. Giugni,
M. N. Lintangpradipto, A. A. Zhumekenov,
A. Y. Alsalloum, J.-H. Min, I. Dursun,
R. Naphade, S. Mitra, I. S. Roqan,
B. S. Ooi, O. F. Mohammed,
E. D. Fabrizio, N. C. Cho,*
O. M. Bakr* 2008088

Domain-Size-Dependent Residual Stress Governs the Phase-Transition and Photoluminescence Behavior of Methylammonium Lead Iodide

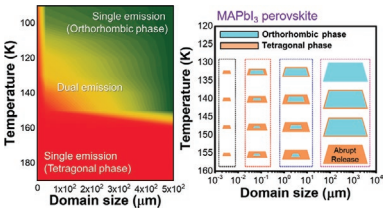

Domain-size-dependent residual stress governs the phase-transition and photoluminescence behavior of $MAPbI_3$ perovskite. Key features in the temperature-dependent photoluminescence and phase-transition behaviors are related to the extent of crystal domain-size-dependent residual stress and stem from the considerable volume difference ($\Delta V \approx 4.5\%$) between the primitive unit cells of the orthorhombic (at 80 K) and tetragonal phases (at 300 K) of $MAPbI_3$.

ADVANCED FUNCTIONAL MATERIALS
www.afm-journal.de

Domain-Size-Dependent Residual Stress Governs the Phase-Transition and Photoluminescence Behavior of Methylammonium Lead Iodide

Kwang Jae Lee, Bekir Turedi, Andrea Giugni, Muhammad Naufal Lintangpradipto, Ayan A. Zhumekenov, Abdullah Y. Alsalloum, Jung-Hong Min, Ibrahim Dursun, Rounak Naphade, Somak Mitra, Iman S. Roqan, Boon S. Ooi, Omar F. Mohammed, Enzo Di Fabrizio, Namchul Cho,* and Osman M. Bakr*

Methylammonium lead iodide ($MAPbI_3$) perovskite has garnered significant interest as a versatile material for optoelectronic applications. The temperature-dependent photoluminescence (TDPL) and phase-transition behaviors revealed in previous studies have become standard indicators of defects, stability, charge carrier dynamics, and device performance. However, published reports abound with examples of irregular photoluminescence and phase-transition phenomena that are difficult to reconcile, posing major challenges in the correlation of those properties with the actual material state or with the subsequent device performance. In this paper, a unifying explanation for the seemingly inconsistent TDPL and phase-transition (orthorhombic-to-tetragonal) characteristics observed for $MAPbI_3$ is presented. By investigating $MAPbI_3$ perovskites with varying crystalline states, ranging from polycrystal to highly oriented crystal as well as single-crystals, key features in the TDPL and phase-transition behaviors are identified that are related to the extent of crystal domain-size-dependent residual stress and stem from the considerable volume difference ($\Delta V \approx 4.5\%$) between the primitive unit cells of the orthorhombic (at 80 K) and tetragonal phases (at 300 K) of $MAPbI_3$. This fundamental connection is essential for understanding the photophysics and material processing of soft perovskites.

1. Introduction

In the past few years, methylammonium lead iodide ($MAPbI_3$)-type halide perovskites, with the general formula AMX_3 (where A = $CH_3NH_3^+$, $CH(NH_2)_2^+$, or Cs^+; M = Pb^{2+} or Sn^{2+}; and X = I^-, Br^-, or Cl^-), have become prominent semiconductors in solar cells, light-emitting diodes, and other optoelectronics.[1–10] The outgrowth in perovskite material technologies is a result of extensive research into the structural (e.g., crystallinity, aging, grain size, chemical impurities, and residual strain) and photophysical (e.g., internal quantum efficiency, exciton binding energy, and charge carrier dynamics)[11–15] properties of the materials, in addition to device engineering. The photoluminescence (PL) and phase-transition behaviors of perovskites have become the primary gauge for the quality of the materials (e.g., defect concentration, impurities, and carrier recombination mechanism) and their

Dr. K. J. Lee, B. Turedi, Dr. A. Giugni, M. N. Lintangpradipto, A. A. Zhumekenov, A. Y. Alsalloum, Dr. I. Dursun, Dr. R. Naphade, Prof. O. F. Mohammed, Prof. E. D. Fabrizio, Prof. O. M. Bakr
Science and Engineering (PSE) Division
King Abdullah University of Science and Technology (KAUST)
Thuwal 23955-6900, Kingdom of Saudi Arabia
E-mail: osman.bakr@kaust.edu.sa

Dr. K. J. Lee, B. Turedi, A. A. Zhumekenov, A. Y. Alsalloum, Dr. I. Dursun, Dr. R. Naphade, Prof. O. M. Bakr
KAUST Catalysis Center (KCC)
King Abdullah University of Science and Technology (KAUST)
Thuwal 23955-6900, Kingdom of Saudi Arabia

Dr. J.-H. Min, Dr. S. Mitra, Prof. I. S. Roqan, Prof. B. S. Ooi
Division of Computer
Electrical and Mathematical Sciences and Engineering
King Abdullah University of Science and Technology (KAUST)
Thuwal 23955-6900, Kingdom of Saudi Arabia

Dr. J.-H. Min, Prof. B. S. Ooi
Photonics Laboratory
King Abdullah University of Science and Technology (KAUST)
Thuwal 23955-6900, Kingdom of Saudi Arabia

Prof. N. C. Cho
Department of energy systems engineering
Soonchunhyang University
Asan 31538, South Korea
E-mail: chon7@sch.ac.kr

The ORCID identification number(s) for the author(s) of this article can be found under https://doi.org/10.1002/adfm.202008088.

DOI: 10.1002/adfm.202008088

Q3 potential performance in devices (e.g., power-conversion efficiency and stability).[15–23]

Published reports provide numerous examples of irregular PL and phase-transition patterns, prompting further research into the elucidation of the origins of such behaviors, including related theoretical proposals.[13,17,20,21,23] In particular, the dual PL peaks and differences observed in orthorhombic-to-tetragonal phase-transition temperatures are critical subjects of debate. The major reason for this inconsistency is the ease with which $MAPbI_3$ perovskites can be fabricated into materials of various spatial orders, such as bulk single-crystals, polycrystals, and nanostructures, depending on the desired application. Therefore, a comprehensive interpretation of the temperature-dependent PL (TDPL) and phase transition needs to account for the potential effects of the crystalline states of the material under study.

Halide perovskites are known as "soft" materials with a relatively small Young's modulus ($G \approx 20$ GPa).[24] Moreover, the phase transition between the orthorhombic and tetragonal phases in $MAPbI_3$ perovskite is accompanied by an abrupt volume change ($\Delta V \approx 2\%$)[25] and is sensitive to both temperature and pressure variations. For example, Capitani et al.[11] induced the appearance of the orthorhombic phase in the $MAPbI_3$ perovskite at room temperature by applying isotropic compression (>1 GPa) with a diamond anvil cell. Interestingly, even after the pressure was released, the system retained the high-pressure orthorhombic phase. A recent study revealed a possible pathway for permanently tailoring the PL properties of perovskite thin films via a suitable substrate-induced lattice mismatch,[26] which also modifies the crystal structure, bandgap, and hole mobility.

In this paper, we present a unifying explanation for the seemingly inconsistent TDPL emission characteristics and the orthorhombic-to-tetragonal phase-transition patterns by examining $MAPbI_3$ materials with a wide range of domain sizes as follows: from polycrystalline (PC) films (<200 nm), highly oriented crystalline (HOC) films (≈70 µm), to single-crystalline (SC) (>1000 µm) structures. The temperature-dependent X-ray diffraction (XRD), PL, and Raman results demonstrate the domain-size-dependent characteristics of $MAPbI_3$ and their traceable stress relaxation dynamics. In particular, accounting for the large volumetric variation induced by the phase transition,[25] shows the mechanism through which the phase transitions occurring between 130 and 170 K[27,28] generate different residual stresses/strains depending on the crystal domain sizes of the samples. The fundamental connection between the dynamics of domain-size-dependent residual stresses and the material's photophysical properties during phase transitions provides an essential framework for understanding these "soft" perovskites and gives a new aspect to consider in their device-oriented processing.

2. Results and Discussion

2.1. $MAPbI_3$ Perovskite with Various Crystalline States

The crystalline state of $MAPbI_3$ perovskite differs as a result of the specific growth technique selected for the final optoelectronic device, ranging from homogeneous bulk single-crystals to inhomogeneous PC thin films or low-dimensional partially oriented structures (e.g., nanowires, quantum dots, and highly ordered crystals).[29–33] To investigate the structural differences between these crystalline states, we selected three archetypal platforms: PC, HOC, and SC $MAPbI_3$ perovskites fabricated through spin-coating,[17,34] temperature-gradient-assisted solidification,[35] and inverse temperature crystallization processes,[36] respectively. **Figure 1**A shows photographs of the three structures and the top-views of scanning electron microscopy images, whereas the inset histograms present their domain-size distributions. The homogeneous SC structure contained the largest domain size (>1000 µm), and the HOC films consisted of mid-sized domains (≈70 µm), whereas the smallest domain size (<200 nm) accompanied by size inhomogeneity characterized the PC films. In terms of crystallinity, the as-prepared SC and HOC samples display only a minimal set of peaks in their XRD patterns as a result of the specific crystal orientation in the diffractometer (Figure 1B). Moreover, the PC films are characterized by a larger number of diffraction peaks, indicating a partial loss in the preferential orientation of the crystal. All the characteristic reflections of $MAPbI_3$ are apparent in the powdered sample's XRD pattern, indicating a complete random orientation and confirming that all prepared $MAPbI_3$ perovskites have the same chemical composition (Figure 1C).

To investigate the phase-transition behaviors of these crystalline states, we examined the temperature-dependent XRD spectra of the three $MAPbI_3$ perovskites from 80 to 300 K (Figure S1, Supporting Information). The physical parameters—2theta peaks and full widths at half maxima (FWHM)—were obtained through a $\chi 2$ minimization routine on a model composed of Gaussian functions. We focused on detecting evidence of residual stress/strain conditions in the three perovskites of various crystalline states because we observed that at the phase transition in $MAPbI_3$. The crystal undergoes a relevant volume expansion ($\Delta V \approx 2\%$) that reaches 4.5% in the temperature range of 80 to 300 K.

Figure 2A shows the temperature-dependent XRD 2theta peaks of the (004) and (242) planes for the as-prepared SC, PC, and HOC ranging from 40° to 42°, which exhibit the relative lattice strain trend of each phase, including before and after the transition temperatures. A decrease in the 2theta value of each XRD peak corresponds to the d-space elongation of the corresponding plane. The (004) and (242) planes display structural interplanar extensions in specific crystal directions with increasing temperature.[28] Figure 2B,C illustrate the (004) and (242) planes in the orthorhombic phase, respectively. In the case of SC perovskite (denoted by blue color), the peak positions of the (004) and (242) planes are proportional to the temperature regardless of their phase, indicating that the linear thermal expansion of lattices in both the orthorhombic and tetragonal phases accompanies the transition. However, the XRD peaks of PC and HOC $MAPbI_3$ perovskites (denoted by red and black colors, respectively) start at different 2theta peak positions and exhibit a non-linear shift with temperature in both phases. In particular, the (004) plane of PC distinctly deviates from linear extrapolations in both phase regions with clear spectral evidence of coexistence in the temperature range near the phase transition (highlighted in yellow). Similar analyses were performed

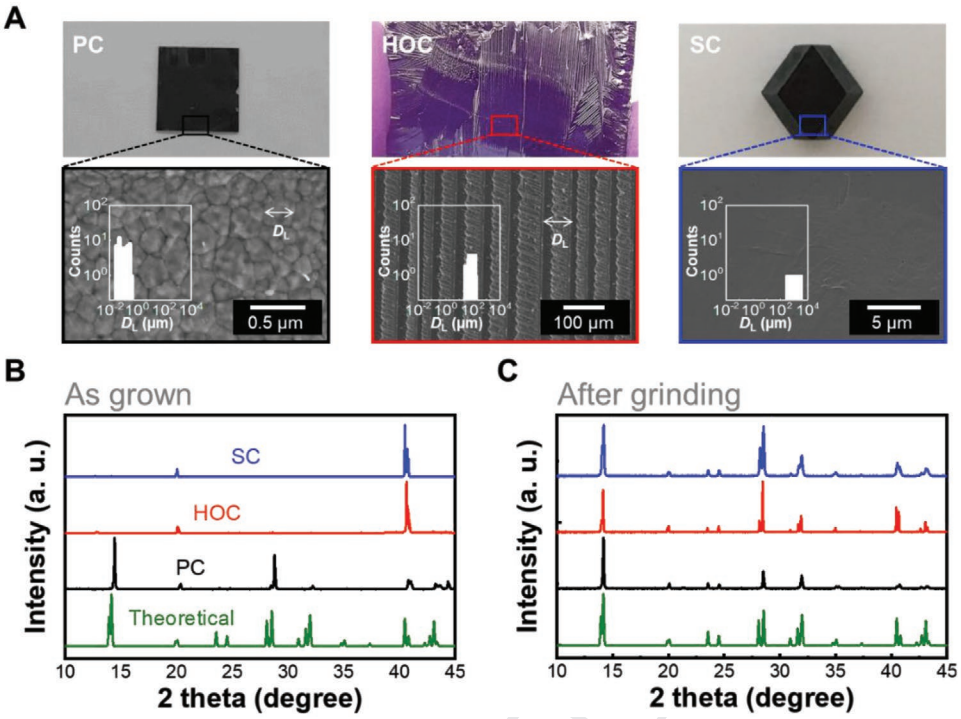

Figure 1. Three crystalline states of $MAPbI_3$ perovskite. A) Photographs and top-view SEM images of polycrystalline (PC) films, highly oriented crystalline (HOC) films, and single-crystalline (SC) $MAPbI_3$ perovskites. Inset: Histograms of domain-size distribution. XRD spectra of PC, HOC, and SC $MAPbI_3$ perovskites in the tetragonal phase at 300 K for B) as-grown and C) ground states.

for other corresponding pairs of crystallographic planes of SC and PC $MAPbI_3$ perovskites (see Figures S2, S3, and S4, Supporting Information). Thus, we deduced that the difference in the degree of thermal lattice expansion accompanying the phase transition in these corresponding planes depends on the different crystalline states of the $MAPbI_3$ perovskites, which are not related to their chemical composition.

To gain further insights into these material-state-dependent deformations, we analyzed the FWHM of the 2theta peaks, which are ≈2.355 of the fitted Gaussian standard deviation σ (Figure S5, Supporting Information). Figure 2D shows the relative FWHM variation of the three $MAPbI_3$ perovskites with temperature for the (004) and (242) planes as $\Delta\sigma(T)/\sigma(100\ K)$. In general, peak broadening is caused by a deviation from the ideal crystalline lattice as a finite crystallite size (Scherrer model), grain surface relaxation, and non-uniform lattice distortions monotonously increasing with temperature (Debye–Waller factor).[37,38] Following the Williamson–Hall model,[39] we expected the pure size effect to be substantially temperature independent, whereas the lattice strain contribution to the

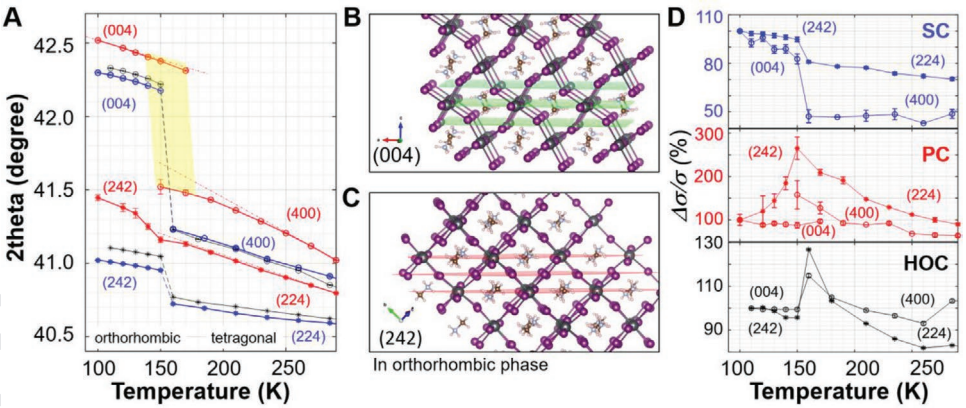

Figure 2. A) Temperature-dependent XRD 2theta peaks of SC (blue color), PC (red color), and HOC (black color) perovskites in the range from 40.5° to 42.5°. Visual illustration of B) the (004) and C) the (242) planes in the orthorhombic phase of SC. D) Variation in FWHM, expressed as $(\Delta\sigma(T)/\sigma(100\ K)\ \%)$ of the temperature-dependent XRD 2theta peaks of SC (blue color), PC (red color), and HOC (black color) perovskites. σ is the Gaussian standard deviation.

linewidth is proportional to a temperature-dependent inhomogeneous strain that we recognized to have a dominant role in the phenomenology of $MAPbI_3$ perovskite.

We measured non-uniform FWHM variations in a rather large temperature range across the transition, indicating interplanar space modulation as a residual stress-strain condition. As mentioned above, the phase transition in $MAPbI_3$ entails significant voluminal deformation, mainly resulting in residual stress or macroscopic cracks, especially for the SC perovskite (see Figure S6 and Video S1, Supporting Information). All samples exhibited a phase transition between 150 and 160 K with considerably different FWHM variation patterns from 80 to 300 K. Based on the FWHM variation, the SC perovskite displayed an abrupt phase transition at a temperature of ≈150 K, which is likely a transient chain reaction. Such deformation dynamics is well-known as a conventional phase transition of crystals (e.g., the rapid phase transition with a sharp increase in the stress at critical temperatures involving either macroscopic fractures or expansion).[40,41] Therefore, the SC perovskite has the ability to rapidly transfer energy, heat, and structural changes through the lattices, which act as a large domain. In contrast, PC $MAPbI_3$ perovskites undergo a series of FWHM changes across the entire temperature range. This change in FWHM variation indicates that the residual stress is constantly changing over the entire temperature range, up to 270% for the (242) plane and exceeding 310% for the (301) plane. These persistent and inhomogeneous changes in the PC $MAPbI_3$ perovskite are likely caused by the inhomogeneity of the domain size or the presence of domain boundaries that locally suppress the volume expansion and phase transition of the domains in the PC perovskite with increasing temperature (approaching the transition). The FWHM variation of HOC exhibits intermediate similarities between these two because HOC has a relatively larger domain size with a lower density of domain boundaries than PC. Owing to the micrometer domain size of HOC, the phase transition occurs at the same temperature as in the SC perovskite (160 K) and does not appear as early as in the PC perovskite (130 K), thus limiting the onset of the domain-size phase transition to a certain crystal size. The inhomogeneity of domain sizes in HOC is relatively less than that of PC; thus, the HOC perovskite produces a small FWHM variation. Moreover, the coexistence of phases was observed in both the HOC and PC, as shown in Figures S2 and S4, Supporting Information. This result corresponds with the findings of Stavrakaz et al.[28] in which a decrease in the onset of the phase-transition temperature and the coexistence of both phases were observed in PC $MAPbI_3$ thin films with decreasing domain sizes. Interestingly, after grinding the three $MAPbI_3$ perovskites into fine powders, the XRD peaks of PC and HOC samples shifted back toward smaller diffraction angles, corresponding to a d-space elongation of up to 0.65% (Figure S7, Supporting Information). This grinding process releases the compressive inter-domain stress and restores the interplanar expansion. Overall, the temperature-dependent XRD results reveal that the crystalline state of $MAPbI_3$ perovskite, especially the domain size and/or the density of domain boundaries, determines the degree of residual strain/stress from the thermal lattice expansion and reconstruction of the lattice, which entails phase transitions of the domains.

Raman investigations of the SC and PC samples confirmed the duality of the stress accumulation observed in our $MaPbI_3$ perovskites, as detailed in Supporting Information. Direct acquisition of the vibrational spectrum on the microscale facilitated specific insights into the lattice rearrangement as a function of temperature, before and after the phase transition. The low wavenumber peaks in the Raman spectra of SC, corresponding to either the cage modes (octahedra twist) or the specific cation modes (nodding donkey near the N atom in the MA),[42] disappeared at temperatures higher than 155 K (Figure S9, Supporting Information), indicating a structural phase transition. In contrast, the SERS spectra collected for the PC sample (Figure S10A, Supporting Information) show multiple peaks that indicate a smooth transition from the orthorhombic-to-tetragonal phases, according to the corresponding emission profile shown in Figure S10B, Supporting Information. In particular, the two bands corresponding to the lurching MA and C—N torsion in the range of 80 to 300 cm^{-1} are higher in intensity in the spectra of the PC $MAPbI_3$ perovskite. Thus, the available space and degrees of freedom of the organic moieties gradually change in the lattice with temperature (broadening and splitting of multiple peaks), resulting in a smooth transition from a trapped state in a given multiconfiguration orientation in the low-temperature phase to a gradually unlocked condition at temperatures above the phase transition.

2.2. Optical Characterization of $MAPbI_3$ Perovskite with Various Crystalline States

We next studied the spectral differences in the TDPL and power-dependent PL (PDPL) patterns of the PC, HOC, and SC $MAPbI_3$ perovskites. The samples were equilibrated for 10 min at each temperature setpoint before the TDPL/PDPL measurements to ensure uniform temperature throughout the material. **Figure 3**A shows the normalized TDPL and PDPL contour maps of the three $MAPbI_3$ perovskites. We noted that each crystalline state consistently exhibited inherent PL contour map patterns. At temperatures below 150 K, the PC $MAPbI_3$ perovskite showed dual PL emission peaks and a spectrum tail in the infrared (IR) region. Trap states cause the spectrum tail of the PC perovskite thin film, and they are clearly activated in the orthorhombic phase in the low-temperature region.[15,16,43] In contrast, the SC $MAPbI_3$ perovskite showed only a single PL emission peak (750 nm at 80 K) without any tail features in the spectrum. The HOC sample shows PL emission features intermediate between those of the PC and SC $MAPbI_3$ perovskites. The TDPL pattern of the HOC $MAPbI_3$ perovskite is similar to that of another PC $MAPbI_3$ perovskite with an average domain size of 100 µm (Figure S13, Supporting Information). Despite all samples being $MAPbI_3$, these differences in TDPL properties were repeatedly and reproducibly observed according to the domain size below 150 K. Above 150 K, all three structures commonly exhibit single PL signals corresponding to the tetragonal phase of $MAPbI_3$ perovskite. However, we cannot exclude the presence of orthorhombic or any other phase that could be optically inactive in this case.

The PDPL contour maps of the as-grown PC, HOC, and SC $MAPbI_3$ perovskites also displayed noticeable differences

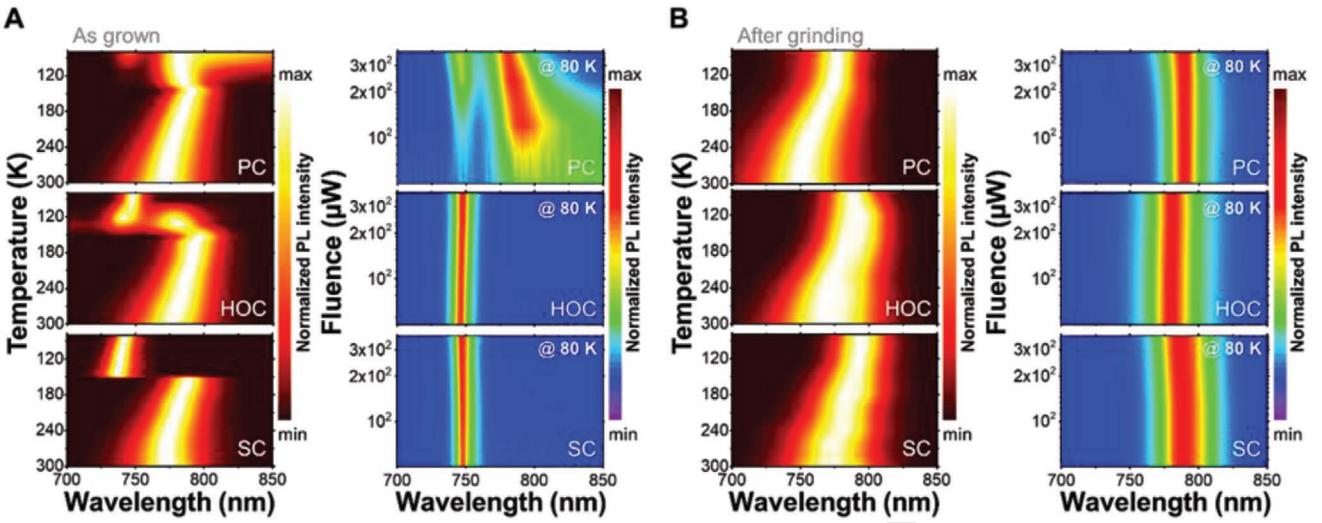

Figure 3. Temperature-dependent photoluminescence (TDPL) and power-dependent photoluminescence (PDPL) contour maps of as-grown PC, HOC, and SC $MAPbI_3$ perovskite A) before and B) after finely grinding.

(Figure 3A). The PC $MAPbI_3$ perovskite shows a dual PL peak at 80 K over the excitation fluence range of 50–370 μW, owing to the coexistence of the orthorhombic and tetragonal phases. In contrast, the HOC and SC samples showed only single PL peaks corresponding to the orthorhombic phase. Based on these spectral results, we deduced that the phase transition from the orthorhombic phase (≈750 nm at 80 K) to the tetragonal phase (≈780 nm at 300 K) proceeds differently in various crystalline states of the $MAPbI_3$ perovskite. Considering our model and expectations, these differences were not surprising when the as-prepared PC, HOC, and SC $MAPbI_3$ perovskites were ground into fine powders (Figure 3B). We performed a fine grinding process to obtain $MAPbI_3$ nanoparticles,[44] as shown in Figure S14, Supporting Information. The PL peak position of each powder was shifted according to the size distribution of the nanoparticles.[45] However, the multiple emission features on the TDPL/PDPL contour maps converge to the same emission pattern, that is, to that of the tetragonal phase. Notably, the tetragonal phase is present even at temperatures below 150 K without undergoing any optically detectable phase transitions. Furthermore, we ground the samples under an inert atmosphere (N_2) to eliminate the effects of possible oxidation or hydration of the perovskite. However, grinding only affected the FWHM of PL (Figure S15, Supporting Information). In fact, the PL properties of ground $MAPbI_3$ perovskites resemble those of $MAPbI_3$ nanocrystals (NCs). Diroll et al.[21] recently demonstrated that $MAPbI_3$ NCs exhibit optical properties distinct from those of the bulk material below 160 K, including no optically detectable phase transitions from the tetragonal to orthorhombic phases. In addition to the PL, visible and IR absorption measurements confirmed that $MAPbI_3$ NCs retained the properties of the tetragonal phase even at temperatures as low as 3 K.[21] These experimental observations indicate that in the absence of domain boundaries, the optical characteristics of $MAPbI_3$ perovskites still depend on the domain size. This relationship is clearly observed in the distinctive PL features of the SCs and powdered samples.

2.3. Optical Characteristics of SC $MAPbI_3$ in the Phase Transition

As demonstrated, unlike other crystalline states of $MAPbI_3$ perovskite, the SC samples undergo an abrupt phase transition between the orthorhombic and tetragonal phases at ≈150 K. To investigate the phase-transition process from the surface to the bulk, we measured the TDPL spectra of the sample using three different excitation wavelengths: 325, 473, and 633 nm. The size of the SC perovskite used in the TDPL measurements was ≈3 mm The penetration depth (δ) in the perovskite structure at these laser lines was calculated to be 19.6, 104.2, and 494 nm, respectively, based on the absorption coefficients reported in the literature.[46] The TDPL contour map for each excitation is magnified over the phase-transition (ΔT_{trans}) temperature range from 135 to 150 K (**Figure 4**A). As mentioned in the previous section, the PL at ≈750 nm corresponds to the orthorhombic phase, whereas the PL at ≈780 nm stems from the tetragonal phase. By increasing the temperature, we observed an evolution of the ratio of the two peaks, which indicates a change in the proportion of the phases. Moreover, we observed different proportions of the two phases at varying penetration depths (Figure 4B). The X–X' isotherm lines reveal that the SC $MAPbI_3$ perovskite remains mostly in the orthorhombic phase at 138 K, whereas its surface is composed of two phases. However, the Y–Y' isotherm lines show that the core of the SC $MAPbI_3$ mainly consists of the orthorhombic phase at 143 K, whereas the surface has a higher ratio of the tetragonal phase. Finally, the Z–Z' isotherm lines indicate the presence of mixed phases in the core of the crystal and the complete conversion of the surface to the tetragonal phase at 148 K. These findings indicate that the phase transition of SC $MAPbI_3$ from the orthorhombic-to-tetragonal phases starts from the crystal (i.e., domain) surface and continues inward toward the crystal (i.e., domain) core, resembling a shrinking core model.[47,48] A surface-triggered phase transition induces this inward propagation of the phase boundary within a narrow temperature region (ΔT_{trans} < 10 K), as illustrated in Figure 4C.

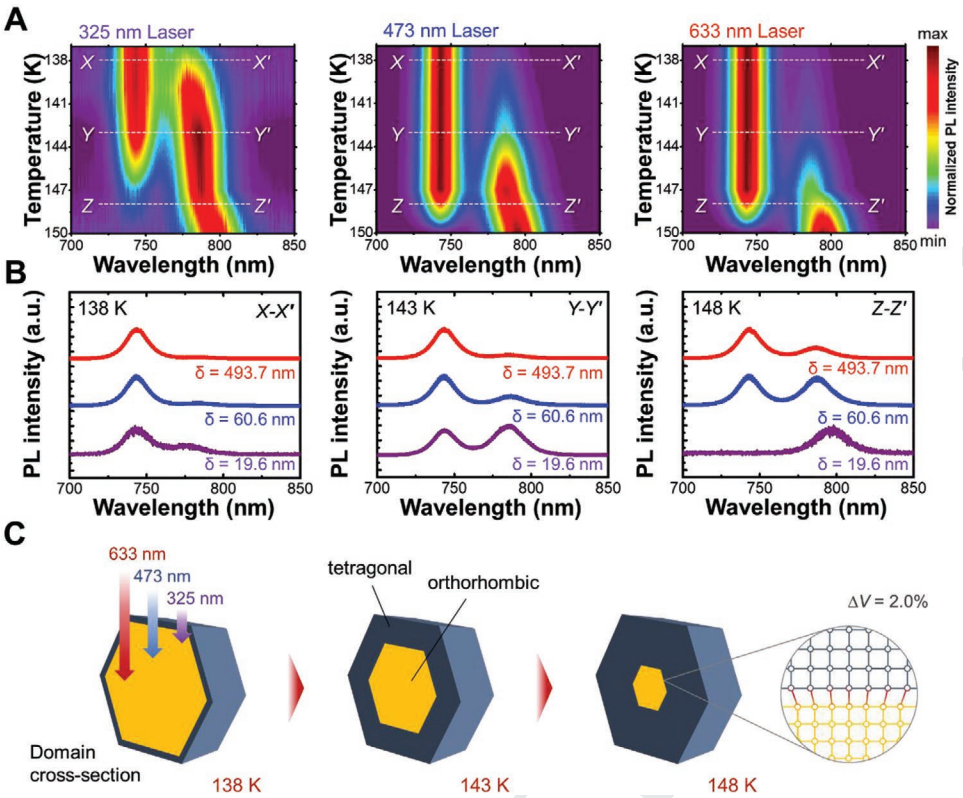

Figure 4. Surface-triggered phase-transition of SC. A) Contour maps of temperature-dependent PL at ΔT_{trans} values ranging from 135 to 150 K as a function of excitation wavelength. B) Depth-dependent PL spectra at 138, 143, and 148 K (*X–X'*, *Y–Y'*, and *Z–Z'* isotherm lines at different penetration depths indicate different ratios of the two phases). C) Illustrations of phase boundary propagation into the crystal core over a small ΔT_{trans} range (<10 K) with increasing temperature.

2.4. Domain-Size-Dependent Optical Characteristics of $MAPbI_3$ Perovskite

To further elucidate the domain-size-dependent phase transition of $MAPbI_3$ perovskite, we selected a number of crystallites from gently crushed SCs with different domain sizes and measured their size and PL spectra at 80 K (**Figure 5**A). For SCs with a domain size smaller than 50 nm, a single PL peak arising from the tetragonal phase was observed. In contrast, for domain sizes between 1 and 300 µm, the crystallites displayed dual PL emission originating from the coexistence of the two phases. Above a domain size of 500 µm, a single PL emission

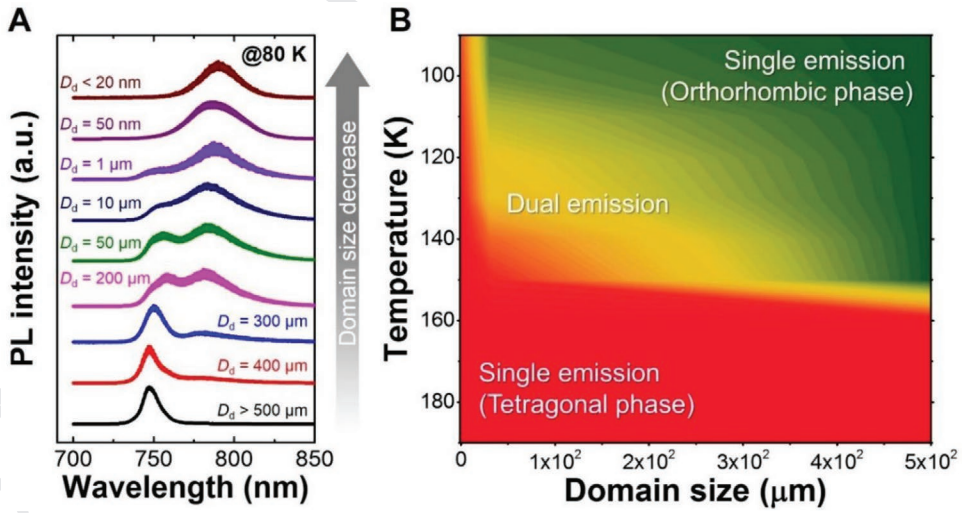

Figure 5. Domain-size-dependent TDPL properties. A) PL spectra at 80 K for $MAPbI_3$ perovskites of different domain-sizes. B) Contour map of the phase-transition process as a function of domain-size for $MAPbI_3$ from 80 to 190 K.

peak arising from the orthorhombic phase was observed. In comparison, Diroll et al.[21] reported the TDPL results for NCs (D_d < 20 nm), showing a tetragonal phase with a single PL peak over the entire temperature range from 10 to 300 K and no phase transition between the tetragonal and orthorhombic phases. Dar et al.[13] reported the existence of two phases in PC $MAPbI_3$ (D_d > 500 nm) that exhibit dual emissions at temperatures as low as 15 K. Diab et al.[14] reported a single orthorhombic phase in SC $MAPbI_3$ (D_d > 2 cm) at 80 K with an abrupt phase transition at 150 K. Similarly, Fang et al.[20] measured the PL of SC $MAPbI_3$ perovskite at 80 K, but observed dual emissions due to D_d < 200 µm. Thus, our observations reconcile the disparate results reported in the literature and demonstrate that at low temperatures, the tetragonal phase becomes more favorable with decreasing domain sizes in $MAPbI_3$ perovskite. Based on this finding, we revealed that regardless of the presence or absence of domain boundaries, as in PC $MAPbI_3$, the optical properties and phase transition are mainly determined by the domain size of perovskite because SC $MAPbI_3$ generates various domain-size-dependent residual stresses. In addition, the difference in the internal residual stress, depending on the domain size, acts as a relative repulsive force, and it could suppress the phase transition that attempts to propagate from the surface to the core of domains, such as in the shrinking core model shown in Figure 4.

Figure 5B summarizes the phase transitions of $MAPbI_3$ perovskites as a function of the domain size. Based on our two observations of a domain-size-dependent phase transition and a surface-triggered phase transition, we present a schematic of the mechanism of the orthorhombic-to-tetragonal phase transition in $MAPbI_3$ perovskite. Specifically, large domains (D_d > 200 µm) are resistant to continuous phase transitions up to relatively high temperatures. However, after reaching a critical point (T_{trans} ≈ 150 K), a complete transition occurs within a short temperature range despite the large domain size. In contrast, intermediate-sized domains (10 µm < D_d < 300 µm) undergo a gradual phase transition over a wide temperature range, with onset temperatures significantly lower than those for larger domains. The elevation of the phase-transition temperature with an increase in the domain size has been observed in other materials.[49] Finally, the smallest domains do not undergo any optically detected phase transition and prefer to maintain the tetragonal phase throughout the entire temperature range. We propose that the unit cell volume change during the phase-transition process creates residual stress between the two phases. This stress increases with the domain size. Thus, SCs with large domains undergo a phase transition at higher temperatures than structures with smaller domains, as the large residual stress of the former resists the transformation. Furthermore, the narrow temperature window of the phase transition of SCs is also a result of the residual stress, which facilitates the transformation for the release of the large-accumulated stress.

2.5. Surface Inhomogeneity of SC $MAPbI_3$ Perovskite by the Aging Effect

One of the general features of SC $MAPbI_3$ is the change in the PDPL emission peaks with aging. **Figure 6**A shows the contour PDPL maps of the SC $MAPbI_3$ perovskite at 80 K according to the degree of exposure to the atmosphere. X-ray photoelectron spectroscopy depth profiling results show carbon rates when the crystallinity of the SC domain is disrupted from the surface through perturbation of the lattice periodicity (Figure S17, Supporting Information). The dual emission PL peaks at low fluences, which became stronger with aging, resembled that of PC perovskite starting from the surface.[50] Further, we split the 3-month-aged SC perovskite in half, and the PDPL of two regions (*i*: surface and *ii*: core) was measured, as shown in Figure 6B. Unlike the surface, the core retained the representative PL characteristics of SC perovskites with a single

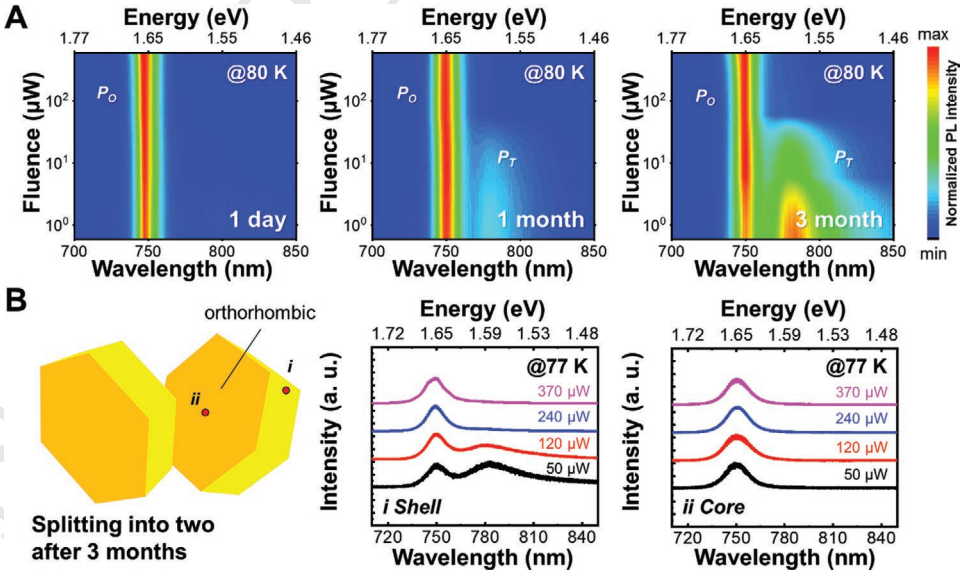

Figure 6. A) Contour PDPL maps of SC $MAPbI_3$ perovskite according to the degree of exposure to the atmosphere. B) PDPL spectra of SC $MAPbI_3$ perovskite exposed to the atmosphere for 3 months: i) surface and ii) core in the orthorhombic phase.

peak emission pattern over the entire fluence range. Such inhomogeneity at the surface accompanies the volume change more quickly than that of the core, resulting in continuous residual stress/strain changes. Thus, these PDPL results could act as a gauge to indicate the crystallinity of the SC perovskites.

3. Conclusions

In conclusion, we demonstrated that various TDPL emission patterns can be attributed to the extent of the domain-size-dependent residual stress of $MAPbI_3$ resulting from the volume difference ($\Delta V = 4.5\%$) between the primitive unit cells of the orthorhombic (at 80 K) and tetragonal (at 300 K) phases. As the temperature increased from 80 to 300 K, the orthorhombic-to-tetragonal phase transition in $MAPbI_3$ perovskite evolved depending on the domain size, which manifested as different temperature-dependent XRD patterns and PL spectra of the $MAPbI_3$ perovskite samples with varying domain sizes. Our work elucidates the seemingly inconsistent TDPL characteristics across different perovskite structures and reveals why the phase-transition variance is responsible for such PL behavior. Domain-size-dependent stress management is thus an essential frontier in the engineering of hybrid perovskite-based devices.

4. Experimental Section

Materials: Chemicals and Reagents: Methylamine (33% in absolute ethanol), *N,N*-dimethylformamide (DMF, ≥99.8%, anhydrous), dimethyl sulfoxide (DMSO, ≥99.9%, anhydrous), and γ-butyrolactone (GBL, ≥99%) were purchased from Sigma Aldrich. Lead (II) iodide (99.999%, ultra-dry) and toluene (≥99.9, anhydrous) were purchased from Alfa Aesar. Formic acid (≥98%) was purchased from Acros Organics. Methylammonium iodide (MAI) was purchased from Greatcell Solar. All chemicals were used without further purification.

Methylammonium Formate Synthesis: The synthesis of methylammonium formate (MAFa) has been previously reported.[51] Briefly, 9.4 g of the methylamine solution was chilled in an ice bath for 5 min with stirring under a nitrogen stream to eliminate oxygen in the flask. Next, 4.6 g of formic acid was mixed with anhydrous absolute ethanol in a 1:1 volume ratio. The formic acid solution was slowly added to the methylamine solution using a syringe pump. After the reaction was completed, the nitrogen stream was removed, and the MAFa mixture was then stirred at room temperature in air for 2 h. Then, the residual solvents were removed by a rotary evaporator to obtain a clear and viscous liquid. The solution was stored in a glovebox and used within 1 week to ensure high reproducibility.

Sample Preparation: The glass substrates were sonicated for 10 min in acetone and isopropanol and plasma-cleaned before the fabrication of PC and HOC $MAPbI_3$ perovskite films. The PC films were spin-coated from a 1.4 M solution of MAI and lead iodide (1:1 molar ratio) in a DMSO and DMF mixture (1:9 volume ratio) at 4000 rpm for 15 s, and 300 µL of toluene was dropped for 6 s before the spin-coating was completed. The films were annealed at 100 °C for 10 min.

The fabrication of HOC $MAPbI_3$ thin films was recently reported by our group.[35] Briefly, PbI_2 and MAI were mixed in a 1:1 ratio, and a mass of the MAFa solvent equivalent to that of the precursors was added and stirred for 1 h at room temperature. The solution was blade-coated onto a glass substrate at room temperature to fabricate an aligned microarray film. The substrate was attached to a metal bar from the edge of the glass substrate using Kapton tape. The sample was covered with a crystallization dish throughout the solidification process to avoid disturbance from the surrounding air. A temperature gradient was applied by heating the sample from the metal to 85 °C. The entire area was covered with centimeter-long microarrays after 2 h of gradient annealing. After directional solidification was completed, the sample was annealed for 2 h at 85 °C on a hot plate under an N_2 atmosphere.

The SCs of $MAPbI_3$ were synthesized by inverse temperature crystallization.[31] A solution of 1 M MAI/PbI_2 was prepared by stirring at 60 °C in GBL. The solution was gradually heated to 110 °C, and SCs of $MAPbI_3$ grew in a few hours to the desired size.

Raman: Raman spectra were collected in a backscattering geometry with a high-resolution WiTEC alpha Raman spectrometer using high-resolution (1800 gr mm^{-1}) and wide spectral range (600 gr mm^{-1}) gratings. The use of the two gratings allowed the authors to collect high-resolution Raman and broadband fluorescence emission from the same sample volume during the phase-transition and for the whole temperature range. The spectrometer was equipped with Bragg volume grating filters to access Stokes and anti-Stokes low wavenumber phonon energies down to 7 cm^{-1}, and a triple Peltier stage cooled charge-coupled device detector (1600 pixel). The measurements were carried out in the range of 80 to 300 K using a gas flow cryostat (Oxford microstatHe) with optical windows that fit under the microscope of the Raman setup. The two samples were thermally connected to the cold finger of the cryostat using silver paint (Figure S8, Supporting Information). The optical source was a 633 nm He-Ne laser line. The laser beam was focused through the cryostat windows onto the sample using long working distance (Zeiss 20×, NA = 0.4 or Zeiss 10×, NA = 0.35) microscope objectives, reaching a minimum diameter spot size of 3 µm. The laser power at the sampled points was maintained below 250 µW for the crystal and 100 µW for the polycrystal to avoid the laser heating effect due to direct laser absorption. In the case of the crystal, the background of each spectrum, obtained after 10 × 300 s integration time, was subtracted with a sixth-order polynomial, resulting in the cited intense emission (Figure S9, Supporting Information). For the PC films, better results were obtained by subtracting with a multi-shaped curve Figure S10, Supporting Information.

Scanning Electron Microscope Measurement: The surface morphology of all three types of perovskites was analyzed using a Zeiss scanning electron microscope (SEM) with the electron beam accelerated at 5 kV.

XPS: The samples were mounted in floating mode to avoid differential charging. Charge neutralization was required for all samples. Binding energies were referenced to the C 1s binding energy of the adventitious carbon contamination, which was taken to be 285.0 eV. XPS studies were carried out on a Kratos Axis Supra spectrometer equipped with a monochromatic Al Kα X-ray source ($h\nu = 1486.6$ eV) operating at 150 W, a multi-channel plate, and a delay line detector in a vacuum of 10^{-9} mbar. All spectra were recorded using an aperture slot measuring 300 µm × 700 µm. Survey spectra were collected using a pass energy of 160 eV and a step size of 1 eV. A pass energy of 20 eV and a step size of 0.1 eV were used to collect high-resolution spectra.

TDPL: The TDPL spectra were characterized using a Horiba JY LabRAM Aramis spectrometer with an Olympus 50× lens in a temperature-controlled Linkam THMS600 stage. A laser excitation source producing light at 325, 473, and 633 nm were used. For all TDPL measurement temperatures, a holding time of 10 min was maintained to ensure a uniform temperature set-point and phase stability in the samples before the measurement.

XRD: XRD patterns were collected on a Bruker AXS D8 powder diffractometer using a Cu Kα1 (λ = 1.5406 Å) source, a step size of 0.02°, and a speed of 0.5 s $step^{-1}$. Temperature-dependent XRD was also performed with the same parameters, but with a temperature-control chamber (LT chamber, TTK450 from Anton Paar GmbH with a software controller). The data was collected while the temperature changed from the lowest to the highest value. Data collection at each temperature was carried out 2 min after reaching the desired temperature to stabilize the structural changes in the materials. The materials were used as-prepared or ground in a mortar if necessary.

Supporting Information

Supporting Information is available from the Wiley Online Library or from the author.

Acknowledgements

K.J.L., B.T., and A.G. contributed equally to this work. The authors gratefully acknowledge the financial support provided by King Abdullah University of Science and Technology (KAUST). This work was also supported by the Soonchunhyang University Research Fund.

Conflict of Interest

The authors declare no conflict of interest.

Data Availability Statement

The data that support the findings of this study are available from the corresponding author upon reasonable request.

Keywords

domain size, $MAPbI_3$, perovskite, photoluminescence, residual stress

Received: September 24, 2020
Revised: December 29, 2020
Published online:

[1] J.-H. Im, C.-R. Lee, J.-W. Lee, S.-W. Park, N.-G. Park, *Nanoscale* **2011**, *3*, 4088.
[2] J. Jagielski, S. Kumar, M. Wang, D. Scullion, R. Lawrence, Y.-T. Li, S. Yakunin, T. Tian, M. V. Kovalenko, Y.-C. Chiu, *Sci. Adv.* **2017**, *3*, eaaq0208.
[3] Y. Wang, X. Li, J. Song, L. Xiao, H. Zeng, H. Sun, *Adv. Mater.* **2015**, *27*, 7101.
[4] Z.-K. Tan, R. S. Moghaddam, M. L. Lai, P. Docampo, R. Higler, F. Deschler, M. Price, A. Sadhanala, L. M. Pazos, D. Credgington, *Nat. Nanotechnol.* **2014**, *9*, 687.
[5] M. Saliba, T. Matsui, J.-Y. Seo, K. Domanski, J.-P. Correa-Baena, M. K. Nazeeruddin, S. M. Zakeeruddin, W. Tress, A. Abate, A. Hagfeldt, *Energy Environ. Sci.* **2016**, *9*, 1989.
[6] E. Strelcov, Q. Dong, T. Li, J. Chae, Y. Shao, Y. Deng, A. Gruverman, J. Huang, A. Centrone, *Sci. Adv.* **2017**, *3*, e1602165.
[7] G. H. Ahmed, J. K. El-Demellawi, J. Yin, J. Pan, D. B. Velusamy, M. N. Hedhili, E. Alarousu, O. M. Bakr, H. N. Alshareef, O. F. Mohammed, *ACS Energy Lett.* **2018**, *3*, 2301.
[8] G. Maculan, A. D. Sheikh, A. L. Abdelhady, M. I. Saidaminov, M. A. Haque, B. Murali, E. Alarousu, O. F. Mohammed, T. Wu, O. M. Bakr, *J. Phys. Chem. Lett.* **2015**, *6*, 3781.
[9] M. N. Lintangpradipto, N. Tsevtkov, B. C. Moon, J. K. Kang, *Nanoscale* **2017**, *9*, 10075.
[10] A. Y. Alsalloum, B. Turedi, X. Zheng, S. Mitra, A. A. Zhumekenov, K. J. Lee, P. Maity, I. Gereige, A. AlSaggaf, I. S. Roqan, *ACS Energy Lett.* **2020**, *5*, 657.
[11] F. Capitani, C. Marini, S. Caramazza, P. Postorino, G. Garbarino, M. Hanfland, A. Pisanu, P. Quadrelli, L. Malavasi, *J. Appl. Phys.* **2016**, *119*, 185901.
[12] K. Wu, A. Bera, C. Ma, Y. Du, Y. Yang, L. Li, T. Wu, *Phys. Chem. Chem. Phys.* **2014**, *16*, 22476.
[13] M. I. Dar, G. Jacopin, S. Meloni, A. Mattoni, N. Arora, A. Boziki, S. M. Zakeeruddin, U. Rothlisberger, M. Grätzel, *Sci. Adv.* **2016**, *2*, e1601156.
[14] H. Diab, G. Trippe-Allard, F. Lédée, K. Jemli, C. Vilar, G. Bouchez, V. L. R. Jacques, A. Tejeda, J. Even, J.-S. Lauret, *J. Phys. Chem. Lett.* **2016**, *7*, 5093.
[15] A. D. Wright, C. Verdi, R. L. Milot, G. E. Eperon, M. A. Pérez-Osorio, H. J. Snaith, F. Giustino, M. B. Johnston, L. M. Herz, *Nat. Commun.* **2016**, *7*, 11755.
[16] R. L. Milot, G. E. Eperon, H. J. Snaith, M. B. Johnston, L. M. Herz, *Adv. Funct. Mater.* **2015**, *25*, 6218.
[17] W. Kong, Z. Ye, Z. Qi, B. Zhang, M. Wang, A. Rahimi-Iman, H. Wu, *Phys. Chem. Chem. Phys.* **2015**, *17*, 16405.
[18] D. Li, G. Wang, H.-C. Cheng, C.-Y. Chen, H. Wu, Y. Liu, Y. Huang, X. Duan, *Nat. Commun.* **2016**, *7*, 11330.
[19] A. Dobrovolsky, A. Merdasa, E. L. Unger, A. Yartsev, I. G. Scheblykin, *Nat. Commun.* **2017**, *8*, 34.
[20] H. Fang, R. Raissa, M. Abdu-Aguye, S. Adjokatse, G. R. Blake, J. Even, M. A. Loi, *Adv. Funct. Mater.* **2015**, *25*, 2378.
[21] B. T. Diroll, P. Guo, R. D. Schaller, *Nano Lett.* **2018**, *18*, 846.
[22] A. P. Schlaus, M. S. Spencer, K. Miyata, F. Liu, X. Wang, I. Datta, M. Lipson, A. Pan, X.-Y. Zhu, *Nat. Commun.* **2019**, *10*, 265.
[23] K. Schötz, A. M. Askar, W. Peng, D. Seeberger, T. P. Gujar, M. Thelakkat, A. Köhler, S. Huettner, O. M. Bakr, K. Shankar, *J. Mater. Chem. C* **2020**, *8*, 2289.
[24] S. Sun, Y. Fang, G. Kieslich, T. J. White, A. K. Cheetham, *J. Mater. Chem. A* **2015**, *3*, 18450.
[25] F. Lehmann, A. Franz, D. M. Többens, S. Levcenco, T. Unold, A. Taubert, S. Schorr, *RSC Adv.* **2019**, *9*, 11151.
[26] Y. Chen, Y. Lei, Y. Li, Y. Yu, J. Cai, M.-H. Chiu, R. Rao, Y. Gu, C. Wang, W. Choi, *Nature* **2020**, *577*, 209.
[27] P. S. Whitfield, N. Herron, W. E. Guise, K. Page, Y. Q. Cheng, I. Milas, M. K. Crawford, *Sci. Rep.* **2016**, *6*, 35685.
[28] C. Stavrakas, S. J. Zelewski, K. Frohna, E. P. Booker, K. Galkowski, K. Ji, E. Ruggeri, S. Mackowski, R. Kudrawiec, P. Plochocka, *Adv. Energy Mater.* **2019**, *9*, 1901883.
[29] H. Tsai, W. Nie, J.-C. Blancon, C. C. Stoumpos, R. Asadpour, B. Harutyunyan, A. J. Neukirch, R. Verduzco, J. J. Crochet, S. Tretiak, *Nature* **2016**, *536*, 312.
[30] K. E. Shulenberger, M. N. Ashner, S. K. Ha, F. Krieg, M. V. Kovalenko, W. A. Tisdale, M. G. Bawendi, *J. Phys. Chem. Lett.* **2019**, *10*, 5680.
[31] S. D. Stranks, G. E. Eperon, G. Grancini, C. Menelaou, M. J. P. Alcocer, T. Leijtens, L. M. Herz, A. Petrozza, H. J. Snaith, *Science* **2013**, *342*, 341.
[32] S. J. Yoon, S. Draguta, J. S. Manser, O. Sharia, W. F. Schneider, M. Kuno, P. V. Kamat, *ACS Energy Lett.* **2016**, *1*, 290.
[33] T. C. Sum, N. Mathews, G. Xing, S. S. Lim, W. K. Chong, D. Giovanni, H. A. Dewi, *Acc. Chem. Res.* **2016**, *49*, 294.
[34] N. J. Jeon, J. H. Noh, Y. C. Kim, W. S. Yang, S. Ryu, S. Il Seok, *Nat. Mater.* **2014**, *13*, 897.
[35] N. Cho, F. Li, B. Turedi, L. Sinatra, S. P. Sarmah, M. R. Parida, M. I. Saidaminov, B. Murali, V. M. Burlakov, A. Goriely, O. F. Mohammed, T. Wu, O. M. Bakr, *Nat. Commun.* **2016**, *7*, 13407.
[36] M. I. Saidaminov, A. L. Abdelhady, B. Murali, E. Alarousu, V. M. Burlakov, W. Peng, I. Dursun, L. Wang, Y. He, G. Maculan, A. Goriely, T. Wu, O. F. Mohammed, O. M. Bakr, *Nat. Commun.* **2015**, *6*, 7586.
[37] S. A. Speakman, *MIT Cent. Mater. Sci. Eng.* **2014**, 3. Q4
[38] T. Matsushita, J. Hayashi, *Phys. Status Solidi A* **1977**, *41*, 139.
[39] G. K. Williamson, W. H. Hall, *Acta Metall.* **1953**, *1*, 22.
[40] D. Vaknin, J. L. Zarestky, J.-P. Rivera, H. Schmid, *Phys. Rev. Lett.* **2004**, *92*, 207201.

[41] M. M. H. Smets, S. J. T. Brugman, E. R. H. Van Eck, P. Tinnemans, H. Meekes, H. M. Cuppen, *CrystEngComm* **2016**, *18*, 9363.
[42] M. A. Pérez-Osorio, R. L. Milot, M. R. Filip, J. B. Patel, L. M. Herz, M. B. Johnston, F. Giustino, *J. Phys. Chem. C* **2015**, *119*, 25703.
[43] M. Karakus, S. A. Jensen, F. D'Angelo, D. Turchinovich, M. Bonn, E. Canovas, *J. Phys. Chem. Lett.* **2015**, *6*, 4991.
[44] A. M. Elseman, M. M. Rashad, A. M. Hassan, *ACS Sustainable Chem. Eng.* **2016**, *4*, 4875.
[45] V. D'Innocenzo, A. R. Srimath Kandada, M. De Bastiani, M. Gandini, A. Petrozza, *J. Am. Chem. Soc.* **2014**, *136*, 17730.
[46] A. M. A. Leguy, P. Azarhoosh, M. I. Alonso, M. Campoy-Quiles, O. J. Weber, J. Yao, D. Bryant, M. T. Weller, J. Nelson, A. Walsh, *Nanoscale* **2016**, *8*, 6317.
[47] V. Safari, G. Arzpeyma, F. Rashchi, N. Mostoufi, *Int. J. Miner. Process.* **2009**, *93*, 79.
[48] S. Yagi, D. Kunni, *Symp. (Int.) Combust.* **1955**, *5*, 231.
[49] J. Liu, L. Chen, H. Yang, Z. Zhang, Y. Wang, *Prog. Nat. Sci.: Mater. Int.* **2019**, *29*, 397.
[50] B. Murali, S. Dey, A. L. Abdelhady, W. Peng, E. Alarousu, A. R. Kirmani, N. Cho, S. P. Sarmah, M. R. Parida, M. I. Saidaminov, *ACS Energy Lett.* **2016**, *1*, 1119.
[51] D. T. Moore, K. W. Tan, H. Sai, K. P. Barteau, U. Wiesner, L. A. Estroff, *Chem. Mater.* **2015**, *27*, 3197.

ADVANCED FUNCTIONAL MATERIALS

Editorial Office:
Wiley-VCH GmbH
Boschstraße 12, 69469 Weinheim
Germany
Tel.: (+49) 6201 606 286
Fax: (+49) 6201 606 510

Email: afm@wiley-vch.de

Reprint Order Form

Manuscript No.: _____
Customer No.: (if available) _____
Purchase Order No.: _____
Author: _____

Charges for Reprints in Euro (excl. VAT), prices are subject to change. Minimum order 50 copies; single issues for authors at a reduced price.

No. of pages	50 copies	100 copies	150 copies	200 copies	300 copies	500 copies
1– 4	345,—	395,—	425,—	445,—	548,—	752,—
5– 8	490,—	573,—	608,—	636,—	784,—	1077,—
9–12	640,—	739,—	786,—	824,—	1016,—	1396,—
13–16	780,—	900,—	958,—	1004,—	1237,—	1701,—
17–20	930,—	1070,—	1138,—	1196,—	1489,—	2022,—
every additional 4 pages	147,—	169,—	175,—	188,—	231,—	315,—

Information regarding VAT: The charges for publication of *cover pictures /reprints/issues/poster/Video abstracts/* are considered to be "supply of services" and therefore subject to German VAT. However, if you are an institutional customer outside Germany, the tax can be waived if you provide us with the valid VAT number of your company. Non-EU customers may have a VAT number starting with "EU" instead of their country code, if they are registered with the EU tax authorities. If you do not have a valid EU VAT number and you are a taxable person doing business in a non-EU country, please provide a certification from your local tax authorities confirming that you are a taxable person under local tax law. Please note that the certification must confirm that you are a taxable person and are conducting an economic activity in your country. **Note:** certifications confirming that you are a tax-exempt legal body (non-profit organization, public body, school, political party, etc.) in your country do not exempt you from paying German VAT.

Please send me send bill me for

☐ no. of reprints

☐ no. of issue
(1 copy: 28 Euro)

☐ high-resolution PDF file (330 Euro excl. VAT)
E-mail address: _____

❖ Special Offer:
If you order 200 or more reprints you will get a PDF file for half price.

Please note: It is not permitted to present the PDF file on the internet or on company homepages.

Cover Posters (prices excl. VAT)
Posters of published covers are available in two sizes:

☐ DIN A2 42 x 60 cm / 17 x 24in (one copy: 39 Euro)

☐ DIN A1 60 x 84 cm / 24 x 33in (one copy: 49 Euro)

Postage for shipping (prices excl. VAT)
overseas +25 Euro
within Europe +15 Euro

_____
Date, Signature

VAT number: _____

Mail reprints / copies of the issue to:
_____
_____
_____
_____
_____

Send bill to:
_____
_____
_____
_____

☐ **I will pay by bank transfer**

☐ **I will pay by credit card**

VISA, Mastercard and AMERICAN EXPRESS
For your security please use this link (Credit Card Token Generator) to create a secure code Credit Card Token and include this number in the form instead of the credit card data. Click here:
https://www.wiley-vch.de/editorial_production/index.php

CREDIT CARD TOKEN NUMBER

						V									

Wiley-VCH GmbH – A company of John Wiley & Sons, Inc. –
Location of the Company: Weinheim – Trade Register: Mannheim, HRB 736569
Managing Directors: Sabine Haag and Dr. Guido F. Herrmann

WILEY-VCH